Sychterz, A. and Smith, I.F.C. "Damage mitigation of near full-scale deployable tensegrity structure through behavior biomimetics" Journal of Structural Engineering, 146 (1), 10.1061/(ASCE)ST.1943-541X.0002470, 2020. http://cedb.asce.org Copyright ASCE

Damage mitigation of near full-scale deployable tensegrity structure through behavior biomimetics

Ann C. Sychterz[1] and Ian F. C. Smith[2]

ABSTRACT

Opportunities to explore new structural behavior are made possible by incorporating sensors and actuators in civil-engineering infrastructure. Using analogies, structural behavior can be improved through the mimicry of a living organism. This is called biomimetics and its study inspires functional goals for structures. While most biomimetic research focuses on geometric forms, this paper describes a study of how behavior goals of active structures can be inspired by nature. Tensegrity structures, a system of struts and cables where mechanisms are stabilized by self-stress, are convenient test structures for active control and adaptation. In this situation, adaptation involves changing the damaged structure to satisfy design requirements as closely as possible. Although adaptation improves structural behavior, the prior state of the structure cannot always be fully restored to satisfy design requirements. Newly enhanced algorithms for control resulting in appropriate of cases for reuse exhibit the behavior-biomimetic characteristics of learning through reducing future execution time. Advanced active-control algorithms improve damage-mitigation performance.

Keywords: Tensegrity structures, adaptive structures, damage mitigation, behavior biomimetics, full-scale testing

INTRODUCTION

The mimicry of a living organism is achieved through analogies and its study is called biomimetics. This can be in terms of form, such as the shape of a bird's wing, or behavior, such as opening

---

[1] PhD, A.M.ASCE, Applied Computing and Mechanics Laboratory (IMAC), School of Architecture, Civil and Environmental Engineering (ENAC), Swiss Federal Institute of Technology (EPFL), CH-1015 Lausanne, Switzerland (corresponding author). Email address: ann@sychterz.com

[2] Professor, F.ASCE, Applied Computing and Mechanics Laboratory (IMAC), School of Architecture, Civil and Environmental Engineering (ENAC), Swiss Federal Institute of Technology (EPFL), CH-1015 Lausanne, Switzerland

of flower pedals. Biomimetics inspires functional goals for structures that can be formulated to assess the ability of the structure to exhibit biomimetic behavior such as learning, self-diagnosis, and damage mitigation. Although biomimetic form has been widely applied and discussed (Pawlyn 2011), there are few studies of biomimetic behavior.

Interest in light-weight structural design in engineering has been gaining momentum over the past decade, with proposals involving new materials, innovative designs and new design criteria such as low life-cycle energy (Senatore et al. 2011). Tensegrity structures are closely-coupled structures composed of bars in compression surrounded by a network of cables (Calladine 1978) (Skelton et al. 2001) (Motro 2011) (Pellegrino and Calladine 1986) (Snelson 2012). Little work has concentrated on control in the context of damage; this is expanded below.

One of the first modern descriptions of an active structure was discussed in the scope of kinetic architecture (Zuk 1968). Since tensegrity members are closely coupled, they provide opportunities for testing advanced control algorithms for deployment (Sultan and Skelton 2003). When tensegrity structures lose self-stress, internal mechanisms might arise, and the structure might become unstable (Calladine and Pellegrino 1991) (Schenk et al. 2007). In order to control the structure, either struts (Amendola et al. 2014) (Averseng and Dubé 2012) or cables (Sultan 2014) have been actuated for shape control. Irregularities in joint construction can severely reduce element stiffness (Cai et al. 2019) and efficacy of active control. Control algorithms have not yet been applied for increasing performance of a deployable tensegrity structure over time.

Examples of deployable tensegrity structures include a telescopic grid (Hanaor 1993) and a five-module tensegrity beam (Bouderbala and Motro 2000). Pinaud et al. (2004) discussed vertical deployment of a small-scale tensegrity tower. This work addressed similar challenges as was encountered with space booms (Furuya 1992) (Tibert 2002) (Furuya 2006) (Liu et al. 2014) (Pellegrino 1995). Additionally, retractable roofs were studied for their deployable behavior (Akgün et al. 2011) (Gantes et al. 1989). Although a portable deployable bridge has been proposed (Averseng and Dubé 2012) there was no control system; this structure required manual prestressing.

Damage mitigation has involved correcting movement due to a change in behavior following the event of a damaged element. Given local loss of equilibrium and progressive system collapse, Shekastehband et. al observed that adaptation resulted in local collapse (Shekastehband et al. 2012). Also noted was that increasing self-stress has a greater effect on edge members than midspan members of a tensegrity structure (Shekastehband et al. 2011). Ashwear and Eriksson (2014) introduced a known perturbation to measure the dynamic response of actively-controlled structures. Ashwear and Eriksson (2017) have also made vibration-based health monitoring simulation studies of a 2D tensegrity structure. Rieffel and Mouret (2018) applied machine learning techniques for damage adaptation to only a small and single module tensegrity structure for locomotion. Mitigation of damaged elements in a deployable tensegrity structure has not yet been studied.

Several researchers have studied adaptation strategies for non-deployable tensegrity structures. Simulated annealing search was compared with a stochastic search method called Probabilistic Global Search Lausanne to find good control commands (Raphael and Smith 2003). Telescopic struts within the structure have been used to control shape and element stress values due to loading (Fest et al. 2004). Although control algorithms change element length for small shape changes, these algorithms were not sufficient for adaptation of a deployable structure undergoing large shape changes.

Learning through improvement of control commands was studied for active control of an adaptive tensegrity structure (Adam and Smith 2006). Control of a tensegrity structure benefitted from reinforcement learning using case-base reuse for self-diagnosis and multi-objective commands (Domer and Smith 2005). The adaptive structure was shown to be damage tolerant due to the active control system. This structure was not deployable.

Several deployment studies of the structure described in this paper then showed that use of springs and continuous cables reduces the number of required actuators and that the structure was suitable for controlled deployment (Rhode-Barbarigos et al. 2012b). Deployment of the tensegrity structure and a search algorithm for midspan connection of the two halves of the structure was developed (Veuve et al. 2015) and reused for adaptation using small movements (Veuve et al. 2017). Spring stiffness influenced the command sequence for deployment (Veuve et al. 2016). Zolesi et al. (2012) analyzed and tested deployment of a tensegrity reflector. Few studies have included experimental work on active control for deployable structures.

While self-diagnosis using dynamic measurements and control algorithms for movement of deployable tensegrity structures has already been developed (Sychterz and Smith 2018b), this paper focuses on learning and damage mitigation. This paper builds on capabilities for damage detection and location using vibration measurements of the tensegrity structure (Sychterz and Smith 2018b). FIG. 1 is a schematic of the biomimetic structure analogy. Behavior of living organisms are on the left and the corresponding functional goals of biomimetic structures are on the right. The aspects surrounded by a thick grey line are the subject of this paper.

This paper contains a description of a development of control strategies for damage mitigation and for improving the effectiveness of this control over time. A description of the near-full-scale tensegrity structure and equipment is given followed by a background section on previously developed algorithms. Testing and newly developed algorithms for damage mitigation and learning through case reuse are then described. Finally, results from testing, a discussion, and conclusions are presented.

NEAR-FULL-SCALE TENSEGRITY STRUCTURE

The topology shown in FIG. 2 is called a "hollow-rope" and it was proposed (Motro et al. 2006) for a pedestrian footbridge. At full-scale, the center opening of the 16 m span bridge would be large enough for pedestrian traffic. At 1/4-scale, the structure is used for laboratory testing, taking advantage of a closely-coupled behavior that deploys along several degrees of freedom, and it is also kinematically indeterminate.

The 1/4-scale laboratory structure is 4 m in length, 1.5 m in height, and 1.5 m in width. The structure is built in two halves that deploy and connect at midspan. The value of the k-class of a tensegrity structure is the maximum number of compression elements connected at any node.

Constructed of four identical k-class 2 modules, the connected tensegrity structure is a k-class 4, two modules per half. Each half is composed of two pentagonal ring modules with a total of fifteen low-stiffness elements (springs), twenty discontinuous cables, thirty struts, and five continuous active steel cables (Bel Hadj Ali et al. 2010) (See FIG. 3). Struts are steel tubes with a diameter of 28 mm, a thickness of 1.5 mm and a length of 1.35 m. Cables are seven braided-steel-strand, 3 mm in diameter. Springs near the supports of the structure have a stiffness value of 2 kN/m and 2.9 kN/m in the rest of the structure (Rhode-Barbarigos et al. 2012b) (Veuve et al. 2015). Each half of the structure weighs approximately 100 kg. Node pairs to be connected are joined sequentially due to self-weight deflection of the structure.

Measurement equipment for both position tracking and element strain are used for this work: optical-tracking markers on the end-nodes, with load cells on continuous cables, and strain gauges on cables and struts. A motion-capture system by OptiTrack© used eight Prime 13® cameras installed on the supports of the structure. These cameras tracked 3-dimensional position and rotation of the five end-nodes of the module with submillimeter accuracy. Measurements from the optical-tracking system clearly showed vibration effects of the structure and small cable-control commands. The software used to collect position tracking information is called Motive 1.10.0 and it is running on a machine with Windows 7 Enterprise. Information is sent through IP.

To capture forces in the continuous cables, HBM© 10 kN 1 mV/V load cells were installed at the end-nodes of the cables. Installed on the discontinuous cables and struts were HBM© 350 $\Omega \pm 0.35\%$ strain gauges. Tensegrity structures require stress in cables for stability. Relaxing stress on cables of the structure makes a mechanism possible for folding and deployment operations (Pellegrino 1990) (Rhode-Barbarigos et al. 2012a). Strain gauges and motor control data are collected by direct wiring to a National Instruments PXI NI 1042Q machine running Windows 7 Enterprise. LabView 2015 32-bit collects data from the PXI machine and the position tracking information through IP. Feedback control uses Matlab R2013a within the LabView code for calculation. Results of calculations determine control commands for the actuators. This equipment is thus configured for efficient closed-loop control.

Discontinuous cables have one segment between two nodes. Along each continuous cable path, there are four segments for each half of the tensegrity structure. Actuation of the structure originates from the motor winding and unwinding of a cable onto a drum at the supports. Deployment is aided by energy stored in springs. Dynamic relaxation was employed for form-finding and static analysis including sliding-friction. Further improvement to the dynamic relaxation algorithm is discussed in Sychterz and Smith (2017) and Bel Hadj Ali (2017).

When active cables are slack at the end of deployment, there is reduced influence over the position of the connected nodes. A path for deployment should be determined so that continuous cables do not become slack. In case of a non-continuous element rupture, locating damage and applying a control command to improve structural behavior is most efficient when there are no slack cables. Control commands are actuation instructions to lengthen or shorten active structural elements. Sudden loss and mitigation of the effects of damaged cables has not yet been tested and simulated on active structures.

A strategy has been developed to determine cable-length changes. A stochastic search algorithm, probabilistic global search Lausanne (PGSL) and an efficient analysis method, dynamic relaxation (DR) were integrated in the program to find good commands and then evaluate stresses and nodal positions from cable-length changes. Without the presence of self-stress, a tensegrity structure would not be stable under service loading (Pellegrino and Calladine 1986). The structure has six independent states of self-stress (Rhode-Barbarigos et al. 2010).

All simulations of the deployable tensegrity structure used in this paper include sliding friction between active cables and intermediate points of contact (Sychterz and Smith 2017). Static friction is included at every intermediate point of contact in the static dynamic relaxation algorithm since the movement of the tensegrity structure is quasi-static. Error-domain model falsification (EDMF), moving-window principal component analysis (MWPCA) and second-order blind identification (SOBI) are implemented to identify changes in the structure.

Feedback control, the optimal rapidly exploring random tree path-planning for a goal position (RRT*-connect), and the soft-constraint algorithm that were originally developed for deployment (Sychterz and Smith 2018a), are adapted in this paper for mitigation following cable rupture events. They are also used to increase performance over time (learning).

BACKGROUND

The following section describes control algorithms that have been previously developed and implemented on the tensegrity structure for the purposes of deployment. In this paper, they are adapted and combined with new strategies for damage mitigation.

Rapidly exploring random tree optimized connect (RRT*-connect)

Path planning algorithms such as rapidly exploring random trees (Kuffner and LaValle 2000), including a quick-convergence extension called RRT informed (RRT*) (Islam et al. 2012), support navigation of a search space around obstacles.

Boundaries of the search space were defined by spaces occupied by current positions of struts and cables to avoid element collision and over-stress. Collision avoidance prevented two struts developing unwanted contact forces in folded and near-folded states. The RRT*-connect algorithm was adapted for this study to employ the dynamic relaxation model of the tensegrity structure with self-weight to check if the nodal point, q_{rand}, corresponds to a configuration in which two structural elements cross each other. In the model, elements were defined by two nodes and by an index that indicated which nodes are connected to form elements.

Since the elements move in space and relative to each other during deployment, the path was discretized into a sequence of intermediate steps for collision and over-stress avoidance. For each step, an initial point and a target point were defined. Points were generated randomly and were defined by the search space. A sensitivity analysis was completed for the number of steps of the RRT*-connect algorithm where the distance to the next point in the tree, ϵ, was a maximum value of 5 cm. This value was confirmed by the increment determined for the sensitivity analysis for the feedback algorithm.

Collision and overstress avoidance of nodes that were not end-nodes, called interior nodes, restricted movement and this influenced the deployment trajectory of end-nodes (FIG. 4). The rectangle defined the outermost boundary of the search space. Control commands of all active cables were the variables of the RRT*-connect algorithm and the objective was expressed as the Euclidean coordinates of the end-nodes. Variables and objectives were tested by applying cable-length changes of the control commands to the dynamic relaxation method of the tensegrity structure to confirm that new nodal positions did not involve collisions and over-stress.

The tree was extended from the start point by adding a new vertex in an optimal direction based on the search space using a greedy algorithm at a maximum radius from the current vertex. In FIG. 4, a new successful point, q_{new}, was added to the tree connected to q_{near}. The new point was in the optimal direction, q_{target}, at a distance, ϵ, which was the control command and the variable of the RRT path-planning algorithm. Positions of struts and cables were reassessed for each new point in the search tree and movement increments were small, addressing geometrical non-linearity of the structure. For further information on RRT*-connect, please refer to Sychterz and Smith (2018a) and this describes an algorithm that combines RRT* (Islam et al. 2012) and RRT-connect (Xu et al. 2013).

Self-stress soft-constraint algorithm

The shape of the tensegrity structure after midspan connection was irregular and not necessarily aligned between the two supports. Irregular performance led to unexpected joint angles and undesirable internal forces. This was not seen as a weakness since a structure in a realistic non-laboratory environment would also have irregular performance. A self-stress algorithm for shape correction was studied to restore performance of the tensegrity structure regardless of position after midspan connection (Sychterz and Smith 2018a).

The algorithm included computation of an objective function value from the normalized nodal position distances and the normalized element internal forces. This configuration was evaluated based on an objective function that was expressed in terms of the difference between distances

d_{current} and d_{design} and a constraint on internal forces, f_{current}. The current element internal force was accepted if the axial forces were less than half of the material yield value, $0.5f_y$. This reflected on an experimental safety factor of 2.0. A soft-constraint algorithm added a condition where a penalty factor, P, of value 1.25 if the element internal force was greater than $0.5f_y$ and less than $0.67f_y$, was applied to the surcharge of the objective function.

Components of the objective function were expressed as follows:

$$C_d = \frac{d_{\text{design}} - d_{\text{current}}}{d_{\text{design}}} \tag{1}$$

If $f_{\text{current}} < 0.5f_y$, then

$$C_f = \frac{0.5f_y - f_{\text{current}}}{0.5f_y} \tag{2}$$

If $0.5f_y < f_{\text{current}} < 0.67f_y$, then

$$C_f = \left(\frac{f_{\text{current}} - 0.5f_y}{0.5f_y}\right) \cdot P + 1 \tag{3}$$

If $f_{\text{current}} > 0.67f_y$, then the control solution was rejected

The objective function was the normalized distance components added to the normalized element internal forces, see EQ. 4 (Sychterz and Smith 2018a). Element axial forces must be relaxed to prepare for the service phase. Although in-service nodal positions of the structure were not exactly as designed, the self-stress phase partially corrected for mis-aligned elements after midspan connection.

$$C = C_d + C_f \tag{4}$$

TESTING AND NEW ALGORITHMS

Damage mitigation

Damage location algorithms (Sychterz and Smith 2018b) and active control algorithms (Sychterz and Smith 2018a) are combined and modified for new adaptation methodology using machine learning through case-reuse. RRT*-connect and soft-constraint algorithms are described in this paper. The RRT*-connect algorithm is enhanced by decreasing the incremental movement to 1 cm and increasing the number of proposed solutions per iteration from 10 to 50 to improve the trajectory for adaptation. The soft constraint algorithm is enhanced by increasing the penalty factor value P to 1.5 since this was effective in maintaining stresses values at approximately 0.5 f_y in this situation.

The strategy is to first identify whether or not the structure has undergone a loss of stiffness due to a damaged element. If the change in natural frequency of the structure in its current state is below the 2σ threshold of the healthy state, then the structure is damaged. Once damage has been detected, the diagnostic algorithm called error-domain model falsification (EDMF) is implemented to locate the region of damage (Sychterz and Smith 2018b). Once damage has been located, adaptation using RRT*-connect and the soft-constraint algorithm reduce the effects of the loss of stiffness in the structure. This is the foundation for the novel use of case-based reasoning for adaptation to reduce computation time for each iteration of mitigation. Mitigation due to damage is tested on four elements, shown in FIG. 5. Cables 26, 41, 66 and 69 are chosen for rupture and mitigation testing.

Since the rupture of some elements produced a strong response in a number of adjacent elements, it is possible that the exact location of the ruptured element is unknown. From the database of simulations for ruptured elements, control commands for the elements that produced a strong response due to rupture are tested on the structure. FIG. 6 shows the testing methodology for mitigation of the effects of a ruptured element. This procedure includes adaptations of path-planning and the soft-constraint algorithms as explained below.

Roman numerals in the text below correspond to the stages in FIG. 6 and numbers shown in brackets in FIG. 6 indicate equations presented in this paper. Nodal coordinates and element stress values are measured for candidate scenarios for the ruptured cable (i). Average vertical downward displacement of the end-nodes is checked against the allowable limits (ii). The limits for the connected structure are prescribed by Swiss code SIA 260. For the half-tensegrity structure, the limits are a minimum between half of the vertical clearance under the structure at midspan, 80 mm, and a vertical downward displacement producing element stress values no more than $0.5 f_y$. If the limits are not satisfied, candidate models of rupture have then to be selected from the initial model set (iii). This requires estimating combined uncertainty in modelling and measurement to define thresholds. The maximum combined uncertainty is estimated to be 31% for the half-tensegrity structure and 17% for the connected tensegrity structure.

The RRT*-connect algorithm is used to compute the cable-length changes that are required to reach the design requirements (iv). The goal state of the structure is the design requirement for the given state of the tensegrity structure. The incremental distance, ϵ, is lowered from 5 cm in its original implementation to 1 cm for better precision since the distance between initial and target positions is much less than during deployment. Further decrease of increment distance increases computation time of the path-planning algorithm without a noticeable increase in performance.

The candidate scenarios are ordered by closeness to measured end-node coordinates (v), the best is selected (vi), and control commands are applied to the dynamic relaxation simulations (vii). Afterwards, the soft-constraint algorithm iterates until simulated element stress values and distance between the current performance and the design requirements are minimized (viii - xix). Although convergence to positions above the performance limits was observed consistently in this study, a maximum of 200 iterations is imposed (xix). Based on the minimum objective function, the control commands from the RRT*-connect algorithm are modified and displacement limits are checked (xxii). Since the connected structure in service is a context where displacement limits need to be satisfied, mitigation is not successful when the maximum number of iterations is reached (xx-xxi, xxiv). If the maximum number of iterations is reached for the half structure (xxiii), the new position of the structure is the best possible.

Control commands are generated by ten iterations of simulation of the RRT*-connect algorithm. The average of these control commands is implemented on the half and connected tensegrity structure for damage mitigation. Additionally, the soft-constraint algorithm is used prior to the RRT*-connect step to ensure that the structure is moved close to the target position while maintaining a low variation of element stress. This step is initiated prior to executing the control commands on the structure.

Half tensegrity structure

For rupture mitigation during deployment, the overall length of the half tensegrity structure is changing between 40 cm and 200 cm. Rupture is assumed to occur at any increment of 20 cm. From these nine positions, Elements 26, 41, 66, and 69 are ruptured one at a time and the control commands determined by the path-planning and soft-constraint algorithm are applied.

During the process of deployment, assessment of the tensegrity structure is simplified to involve only the ultimate limit state since there is no in-service loading. However, the positions of struts and cables relative to one another are changing during deployment and this increases mitigation difficulty since element collision and overstress need to be avoided regardless of the deployment stage.

Rupture of a cable involved the release of an electro-magnet fitted on the cable. Results for rupture of Element 26 are available for overall structure lengths of 160 cm to 200 cm and of Element 66 for overall structure lengths of 100 cm to 200 cm. At other lengths, initial tension values were too high to ensure safe testing. The deployment sequence is paused, control commands are executed to return the structure to the design requirements for the given overall structure length, and deployment then resumes.

The following observations are made for testing of damage mitigation in folded states, mid-deployment, and near midspan connection. Implementing the RRT*-connect algorithm for mitigation of the effects of a ruptured element during deployment ensures that collision and overstress are avoided.

Although mid-way through deployment there is no longer a possibility of element collision, control of active cables is a challenge as the overall structure length increases. As the tension values in active cables decreases, control over end-node positions becomes coupled, where actuation of one cable affects the position of other end-nodes, and cable-length changes are less effective than when the structure is in the folded state.

When the two halves of the tensegrity are near midspan connection, many cables on the lower half of the structure carry little to no tension. When cables carry no tension, cable-length changes are not effective and other active cables are needed to move the structure. Active control is useful to change the shape of the tensegrity structure to reduce member stresses and vertical downward displacement caused by a damaged element prior to midspan connection. Though the response improves the condition of the structure, the tensegrity structure often cannot be fully restored to its state prior to damage.

Learning using case-based reasoning during deployment

For this study, a case is composed of two vectors representing the direction of actuation for mitigation and actuation commands for mitigation. The correction vectors (0,0,1), (0,1,1), (0,-1,1), (1,0,1), (-1,0,1), (1,1,1), (1,-1,1), (-1,1,1), and (-1,-1,1) are in the form of (x,y,z) where x is the longitudinal direction, y is the transverse direction, and z is the vertical direction. FIG. 7 shows a schematic of vectors for correction of movement of the tensegrity structure towards the design requirement.

FIG. 8 shows the procedure for performance mitigation due to cable rupture during the deployment of the half tensegrity structure using case-based reasoning. Numbers shown in brackets in FIG. 8 indicate equations presented in this paper. Cable-length changes (i) and nodal coordinates (ii) for previous command cases are the inputs for mitigation due to cable rupture in FIG. 6.

Firstly, the Euclidean coordinates are used to calculate the distance between the five end-node positions prior, v_{prior}, and following a damage event, v_{damage}, in 3-dimensions (EQ. 5).

$$v_{vector} = v_{damage} - v_{prior} \tag{5}$$

This produces a vector, v_{vector}, of the difference between the damaged state and the prior state in three dimensions. The average of vectors from all end-nodes yields one vector representing the average change in movement due to a damage event. Normalization of this vector was calculated by dividing the three components of the vector by the absolute value of the greatest number in the vector (EQ. 6).

$$v_{normalized} = v_{vector}/|\max(v_{vector})| \tag{6}$$

In this way, the vectors are normalized, $v_{normalized}$ on the interval [-1, 1] for each dimension (iii). Cases are added to the case-base by comparing the normalized vector with the correction vectors. The normalized vector from measurement is added to the case with the smallest calculated Euclidean distance. Actuation commands from measurement are normalized on the interval [-1, 1] (iv) using the same process as for the normalized vectors and are linked with the given case. When there is more than one entry in a case, the average is taken of the control command for all entries in that given case. All cable rupture cases are tested (v).

The cases are initially created with results of simulated ruptures of discontinuous cables in the half tensegrity structure (vi). Since tension values of cables on the structure were high, experimental cable removal was not possible. Normalized vectors and actuator commands from measured rupture events of Element 26, Element 41, Element 66, and Element 69 were compared with simulation results. Simulated rupture events of discontinuous cables were used as the initial population for cases.

Keeping previous control commands in a cumulative average for each correction vector was more effective than replacing cases to generate control commands. Measured normalized correction vectors of the half tensegrity structure following cable rupture were well-distributed amongst possible case-base entries.

When a new measurement is introduced (vii), case retrieval is completed in the same way as was done with the initial population of measurements. The vector from measurements is normalized and compared with the correction vectors (viii). The cable-length changes are scaled using the normalization factor of the new nodal coordinates (xi). Actuator commands linked with the selected correction vector are retrieved and applied to the structure (x).

Cable-length changes are executed if the new cable-length changes result in performance that is within the limits for the connected and half-tensegrity structure (xi). When a new data entry does not conform to the behavior in the case-base, a check is performed to determine whether or not nodal coordinates are within displacement limits. The case is adapted to the new cable-length changes by implementing the soft-constraint algorithm (xii). This new set of actuator commands are then normalized and are included in the cumulative mean for the selected case (xii), and this results in an improved case-base of control commands for adaptation (xiii).

Connected tensegrity structure

If both halves of the tensegrity structure are connected, changes in nodal positions following a rupture of an element are greatly reduced in comparison to the behavior of the half tensegrity structure. Additionally, active cables in a connected structure carry higher tension than when the structure is not connected. Even though changes in nodal position are low when the structure is connected, perturbation due to a ruptured element has a greater impact on the load path and overall stress level in elements. Therefore, in the event that rupture of an element causes a larger than the average change of nodal positions, fully restoring the connected structure to its prior state may not be possible.

The Swiss code SIA 260 Annex C for pedestrian and cyclist bridges states that near-permanent deflections should be no greater than $L/700$ where L is the bridge span length. For frequent occurrences, the deflection limit is relaxed to 5 mm for design verification and $L/600$ for comfort. For the tensegrity structure scaled to a span of 4 m, the minimum allowable deflection is 5 mm and the maximum allowable deflection is 6.7 mm.

The connected tensegrity structure is more statically indeterminate than the half tensegrity structure. Compared with the half tensegrity, vertical displacement following cable rupture is lower and midspan positions change less following rupture of elements. The implication for mitigation of damage is simplified so that only midspan nodal positions are considered.

RESULTS

Half tensegrity structure

FIG. 9 shows vertical displacement of midspan nodes (negative for downwards movement) in mm for rupture of Element 41 averaged over five tests with an overall structure length of 140 cm. Measured values are shown with a solid line and the simulated result is shown with a dashed line. Variation of two standard deviations, 2σ, is shown for measurements as a light grey band.

Simulation results showed that the control command restores the structure safely to the original position. The element stress values are not exceeded. In simulation, the cable rupture consistently resulted in a smaller vertical downward displacement than measured during testing. FIG. 9 shows the average vertical displacement of the half tensegrity structure for five tests of approximately 18 mm after rupture event and mitigating control commands result in end-node vertical displacement of approximately 6.5 mm. Combining RRT*-connect and the soft-constraint algorithm is useful for reducing the vertical displacement of the tensegrity structure following damage even though simulation results are not close to experimental values. The frameworks using RRT*-connect and the soft-constraint algorithms developed in this paper for case reuse have potential to be applied to other active structures and this is the subject of current research.

A summary of control commands for cable-length changes by application of the RRT*-connect algorithm and the soft-constraint algorithm on the half tensegrity structure are shown in TABLE 1. The mean cable-length changes of the active cables for each ruptured element event are shown. At final deployment stages of the tensegrity structure, longer cable-length changes are required for mitigation of damage. In addition to increased cable-length changes, control commands have more variation with greater overall deployment length between active cables for one rupture event as well as between rupture events of Elements 26, 41, 66 and 69. Following rupture, the deployment sequence is paused, control commands return the structure to the design requirements for the given overall structure length, and deployment then resumes.

TABLE 2 shows the measured vertical displacements after mitigation. Rupture events that produce large vertical deflections, Element 26 and Element 66, could not be completed for deployment lengths of 40 cm to 140 cm and 40 cm to 80 cm respectively due to risk of plastic deformation of the structure. These elements carry a higher tension value than Element 41 and Element 69. Vertical displacement following rupture is the greatest at full length of the half tensegrity structure.

Results from the RRT*-connect algorithm show that control commands for cable-length changes are nonlinearly related to the overall structure length. When the tensegrity structure is in a folded state, dynamic movement due to cable rupture is similar to that of a rigid body. However, in a deployed state, the half tensegrity structure is more flexible than in the folded state and has a response that is similar to a cantilever beam. Cable-length changes for mitigating damage have less variation for overall structure lengths when in the folded state. Variation between cable-length changes of cable rupture events is high due to the high variation of cable tension values of Element 41 (low) and Element 26 (high).

FIG. 10 shows the percent mitigation, the ratio of vertical downward displacement after mitigation relative to the vertical downward displacement after cable rupture of Elements 26, 41, 66, and 69 (EQ. 7).

$$\text{Percent mitigation} = \frac{\Delta z_{restore}}{\Delta z_{damage}} \cdot 100\% \tag{7}$$

Percent mitigation is calculated by the ratio, multiplied by 100, of vertical displacement that is restored after damage, $\Delta z_{restore}$, to the vertical displacement due to damage, Δz_{damage}.

Rupture of cables with high tension values produces large vertical displacements at most overall structure lengths. Greater cable-length changes than the results of the simulation with the RRT*-

connect algorithm are required. In these situations, the soft-constraint algorithm was not able to modify control commands further to consistently reach the vertical downward displacement limit of the half-tensegrity structure.

Tension values of Element 41 and Element 69 are lower than that of Element 26 and Element 66. Mitigation of rupture of Element 41 is a minimum of 37% (140 cm) and 35% for Element 69 (80 cm). Throughout the process of deployment, mitigation of Element 41 and Element 69 rupture events are more consistently feasible than mitigation of Element 26 and Element 66 rupture events, except near the very end of deployment when Element 66 ruptures. For the deploying half-tensegrity structure, damage mitigation allows for successful deployment of damaged structures in situations where damage without mitigation would prevent deployment. While mitigation does not usually lead to full recovery of the extra deflection caused by damage, mitigation between 27% and 84% was sufficient to continue deployment. Vertical downward displacement from all cable rupture events were less than the limit for the half-tensegrity structure. Downward vertical displacement after mitigation was often less than the uncertainty margin of 1 cm for successful operation of the electromagnet connections at midspan (Sychterz and Smith 2018a). The combination of the RRT*-connect algorithm following damage sufficiently reduces the vertical downward displacement of damaged structures so that deployment can proceed successfully.

Learning using case-based reasoning during deployment

Reuse of control cases through case-based reasoning has the potential to reduce execution time for subsequent control-command calculations. Initial entries to the case-base are the results of simulated rupture events. Simulated values of the rupture of Element 26, Element 41, Element 66, and Element 69 initially populate the cases. To compare measurements with the cases, 135 tests, four rupture cables with five tests each for various stages of deployment (see TABLE 2) are used. Actuator commands were retrieved and the soft-constraint algorithm was implemented to reduce deflection.

Results from the initial entries using simulated values are shown in TABLE 3. Control commands following the process in FIG. 8 are shown for damage mitigation of the half tensegrity structure. Only one correction vector, (1,1,1) contained no cases from measurement.

Evolution occurs as the number of entries to the case-base increases and control commands for a new instance of a case are combined in the cumulative mean of the existing control commands. The lengths of control commands are short with little risk of element collision and overstress. Previous work (Adam and Smith 2008) on reinforcement learning proposed removing cases that were retrieved and replacing them with new modified cases. However, for the deployable tensegrity structure, keeping all retrieved cases helps build a more comprehensive case-base. When the structure is deploying or fully connected at midspan, cable-length-changes are more coupled than in the folded state. Additionally, uncertainties are greater in the deployable tensegrity structure than with previous adaptive tensegrity structures. Therefore, a case-base is useful to correlate the effect of a damaged element to the average cable-length change for correction of the structure shape.

TABLE 4 contains a summary of the time required per entry to determine of cable-length changes with no previous information and with learning using case-based reasoning. Application of case-based reasoning reduces the time necessary for calculation and implementation of mitigation commands. As the number of entries in the case-base increases, n, the time of execution for each subsequent iteration decreases. Execution time for control commands occurs at an average speed of 2 s/cm for a cable-length change of l in cm. The number of executions for mitigation for control commands and soft-constraint algorithm are dependent on the number of active cables.

FIG. 11 shows time per entry to determine control commands for learning through case-based reasoning. Repeated events involving the same cable rupture result in a progressive reduction of the time required for finding the best control command.

Execution time for mitigation using learning is reduced by at least thirty times when case-based reasoning is implemented. Modification of control commands resulting in convergence of cases for reuse exhibits the behavior biomimetic characteristic of learning through reducing future execution time.

TABLE 5 shows vectors used to correct the position of the structure that are closest to the movement caused by rupture events during stages of deployment. In the folded state, the vectors are more similar to each other than in the deployed state.

Connected tensegrity structure

For mitigation of damage of the connected tensegrity structure, continuous and discontinuous cables have medium to high tension values following prestress relaxation. TABLE 6 shows the mean cable-length changes of the five active cables using the RRT*-connect algorithm and the soft-constraint algorithm as a check for element stresses. When no damage occurs, no cable-length changes are required. The variation of 2σ is shown for cable-length changes during the five tests of each cable rupture event.

TABLE 7 shows the vertical displacements measured by rupture of Element 26, Element 41, Element 66, and Element 69 for the connected tensegrity structure. Vertical downward displacements for the connected tensegrity structure are less than those of the half tensegrity structure. The last row shows the performance of mitigation due to each element rupture event compared with the serviceability limit of 6.7 mm where only the rupture event of Element 26 exceeded that limit.

FIG. 12 shows percent mitigation of vertical downward displacement for rupture of Element 26, Element 41, Element 66, and Element 69 the connected tensegrity structure.

For the connected structure, damage mitigation between 36% and 86% was sufficient to satisfy code deflection requirements. With the exception of Element 26, structures having cable rupture events are successfully adapted to satisfy the Swiss code for serviceability related to displacement at midspan of $L/600$. Path-planning and constraint-based algorithms successfully enable damage mitigation, in most cases meeting serviceability limits in cases of rupture of discontinuous cables in this structure.

DISCUSSION

Variation in control commands for the half tensegrity structure increases with the overall structure length. Since tension values in cables are less similar in the deployed state than in the folded state, the RRT*-connect algorithm successfully compensates for this variation.

Calculation of cable-length changes through case-based reasoning reduces the execution time and avoids unnecessary cable-length changes. With increasing number of executions, use of the cumulative mean from the case base allows the structure to move towards the pre-rupture performance more effectively than active control without case-based reasoning.

Vertical downward displacements due to cable rupture are larger for the half structure than for the connected tensegrity structure. Effectiveness of mitigation using the RRT*-connect algorithm understandably depends on cable tension values prior to the rupture event. Advanced active control algorithms improve the damage-mitigation performance of the deployable tensegrity structure for the half-tensegrity structure and the connected structure.

There are limitations to tests conducted on the tensegrity structure. Testing was performed only in the context of complete damage of discontinuous cables. Although simulation results show that it is possible to deploy the bridge with one damaged active cable, the element stresses are beyond the threshold of 0.67 f_y (see section "Self-stress soft-constraint algorithm") to conduct a non-destructive test safely with the tensegrity structure. While mitigation of strut damage is not impossible, this was not studied due to testing-safety considerations.

CONCLUSIONS

Living organisms heal when hurt and then learn to improve the next time an injury happens. This functionality has inspired a biomimetic study of damage mitigation and improving adaptation of an active tensegrity structure. Newly enhanced versions of path-planning and soft-constraint algorithms successfully enable damage mitigation in cases of rupture of discontinuous cables in this structure. For the deploying half-tensegrity structure, damage mitigation allows for successful deployment of damaged structures in situations where damage without mitigation would prevent deployment. While mitigation does not usually lead to full recovery of the extra deflection caused by damage, mitigation between 27% and 84% was sufficient to continue deployment. Modification of control commands through modified versions of RRT*-connect, soft-constraint algorithm with case reuse exhibits the characteristic from behavior biomimetics of learning through progressively reducing future execution time by at least thirty times. For the connected structure, damage mitigation between 36% and 86% was sufficient to satisfy code deflection requirements. The framework using the newly-modified RRT*-connect and the soft-constraint algorithms developed in this paper for mitigation and case reuse have potential to be applied to other active structures and this is the subject of current research.

ACKNOWLEDGEMENTS

The research is sponsored by funding from the Swiss National Science Foundation under project number 200020_169026.

APPENDIX I. REFERENCES

Adam, B. and Smith, I. F. C. (2006). "Learning, self-diagnosis and multi-objective control of an active tensegrity structure." *Solid Mechanics and its Applications*, 140, 439–448.

Adam, B. and Smith, I. F. C. (2008). "Reinforcement learning for structural control." *Journal of Computing in Civil Engineering*, 22(2), 133–139.

Akgün, Y., Gantes, C. J., Sobek, W., Korkmaz, K., and Kalochairetis, K. (2011). "A novel adaptive spatial scissor-hinge structural mechanism for convertible roofs." *Engineering Structures*, 33(4), 1365–1376.

Amendola, A., Carpentieri, G., de Oliveira, M., Skelton, R., and Fraternali, F. (2014). "Experimental investigation of the softening stiffening response of tensegrity prisms under compressive loading." *Composite Structures*, 117(11), 234–243.

Ashwear, N. and Eriksson, A. (2014). "Natural frequencies describe the pre-stress in tensegrity structures." *Computers & Structures*, 138(02), 162–171.

Ashwear, N. and Eriksson, A. (2017). "Vibration health monitoring for tensegrity structures." *Mechanical Systems and Signal Processing*, 85, 625–637.

Averseng, J. and Dubé, J. (2012). "Design, Analysis and Self Stress Setting of a Lightweight Deployable Tensegrity Modular Structure." *Procedia Engineering*, 40(7), 14–19.

Bel Hadj Ali, N., Rhode-Barbarigos, L., Pascual Albi, A., and Smith, I. F. C. (2010). "Design optimization and dynamic analysis of a tensegrity-based footbridge." *Engineering Structures*, 32(11), 3650–3659.

Bel Hadj Ali, N., Sychterz, A. C., and Smith, I. F. C. (2017). "A dynamic-relaxation formulation for analysis of cable structures with sliding-induced friction." *International Journal of Solids and Structures*, 127, 240–251.

Bouderbala, M. and Motro, R. (2000). *Folding Tensegrity Systems*. Springer Netherlands, Dordrecht, 27–36.

Cai, J., Yang, R., Wang, X., and Feng, J. (2019). "Effect of initial imperfections of struts on the mechanical behavior of tensegrity structures." *Composite Structures*, 207, 871–876.

Calladine, C. R. (1978). "Buckminster Fuller's "Tensegrity" structures and Clerk Maxwell's rules for the construction of stiff frames." *International Journal of Solids and Structures*, 14(2), 161–172.

Calladine, C. R. and Pellegrino, S. (1991). "First-order infinitesimal mechanisms." *International Journal of Solids and Structures*, 27, 505–515.

Domer, B. and Smith, I. F. C. (2005). "An active structure that learns." *Journal of Computing in Civil Engineering*, 19(1), 16–24.

Fest, E., Shea, K., and Smith, I. F. C. (2004). "Active tensegrity structure." *Journal of Structural Engineering*, 130(10), 1454–1465.

Furuya, H. (1992). "Concept of deployable tensegrity structures in space applications." *International Journal of Space Structures*, 7(2), 143–151.

Furuya, H. (2006). "Concept of Inflatable Tensegrity for Large Space Structures." *ASME Structure, Structural Dynamics, and Materials Conference, Newport, Rhode Island USA*, number May, 1—-9.

Gantes, C. J., Connor, J. J., Logcher, R. D., and Rosenfeld, Y. (1989). "Structural analysis and design of deployable structures." *Computers and Structures*, 32(3-4), 661–669.

Hanaor, A. (1993). "Double-layer tensegrity grids as deployable structures." *International Journal of Space Structures*, 8(1-2), 135–143.

Islam, F., Nasir, J., Malik, U., Ayaz, Y., and Hasan, O. (2012). "RRT*-Smart: Rapid convergence implementation of RRT* towards optimal solution." *2012 IEEE International Conference on Mechatronics and Automation, ICMA 2012*, 1651–1656.

Kuffner, J. and LaValle, S. (2000). "RRT-connect: An efficient approach to single-query path planning." *Proceedings 2000 ICRA. Millennium Conference. IEEE International Conference on Robotics and Automation. Symposia Proceedings (Cat. No.00CH37065)*, 2(Icra), 995–1001.

Liu, Y., Du, H., Liu, L., and Leng, J. (2014). "Shape memory polymers and their composites in aerospace applications: a review." *Smart Materials and Structures*, 23(2), 023001.

Motro, R. (2011). “Structural morphology of tensegrity systems.” *Meccanica*, 46(1), 27–40.

Motro, R., Maurin, B., and Silvestri, C. (2006). “Tensegrity rings and the hollow rope.” *IASS symposium Beijing, China*.

Pawlyn, M. (2011). *Biomimicry in architecture*, Vol. 15. Riba Publishing London.

Pellegrino, S. (1990). “Analysis of prestressed mechanisms.” *International Journal of Solids and Structures*, 26(12), 1329–1350.

Pellegrino, S. (1995). “Large retractable appendages in spacecraft.” *Journal of Spacecraft and Rockets*, 32(6), 1006–1014.

Pellegrino, S. and Calladine, C. (1986). “Matrix analysis of statically and kinematically indeterminate frameworks.” *International Journal Solids Structures*, 22(4), 409–428.

Pinaud, J.-P., Solari, S., and Skelton, R. E. (2004). “Deployment of a class 2 tensegrity boom.” *Smart Structures and Materials 2004: Smart Structures and Integrated Systems*, Vol. 5390, San Diego, CA, USA, SPIE, 155–162.

Raphael, B. and Smith, I. F. C. (2003). “A direct stochastic algorithm for global search.” *Applied Mathematics and computation*, 146(2), 729–758.

Rhode-Barbarigos, L., Ali, N., Motro, R., and Smith, I. F. C. (2012a). “Design aspects of a deployable tensegrity-hollow-rope footbridge.” *International Journal of Space Structures*, 27(2-3), 81–95.

Rhode-Barbarigos, L., Hadj Ali, N., Motro, R., and Smith, I. F. C. (2010). “Designing tensegrity modules for pedestrian bridges.” *Engineering Structures*, 32(4), 1158–1167.

Rhode-Barbarigos, L., Schulin, C., Ali, N., Motro, R., and Smith, I. F. C. (2012b). “Mechanism-based approach for the deployment of a tensegrity-ring module.” *Journal of Structural Engineering*, 138(4), 539–548.

Rieffel, J. and Mouret, J.-B. (2018). “Adaptive and resilient soft tensegrity robots.” *Soft Robotics*, 5(3), 318–329.

Schenk, M., Guest, S., and Herder, J. (2007). “Zero stiffness tensegrity structures.” *International*

Journal of Solids and Structures, 44(20), 6569–6583.

Senatore, G., Duffour, P., Hanna, S., and Labbe, F. (2011). “Pumping vs. iron: Adaptive structures for whole life energy savings.” *Proceedings - 2011 7th International Conference on Intelligent Environments, IE 2011*, 114–121.

Shekastehband, B., Abedi, K., and Chenaghlou, M. (2011). “Sensitivity analysis of tensegrity systems due to member loss.” *Journal of Constructional Steel Research*, 67(9), 1325–1340.

Shekastehband, B., Abedi, K., Dianat, N., and Chenaghlou, M. (2012). “Experimental and numerical studies on the collapse behavior of tensegrity systems considering cable rupture and strut collapse with snap-through.” *International Journal of Non-Linear Mechanics*, 47(7), 751–768.

Skelton, R. E., Adhikari, R., Pinaud, J.-P., and Chan, W. L. (2001). “An introduction to the mechanics of tensegrity structures.” *Conference on Decision and Control*, Orlando, Florida, USA, 4254–4259.

Snelson, K. (2012). “The art of tensegrity.” *International Journal of Space Structures*, 27(2-3), 71–80.

Sultan, C. (2014). “Tensegrity deployment using infinitesimal mechanisms.” *International Journal of Solids and Structures*, 51(21-22), 3653–3668.

Sultan, C. and Skelton, R. (2003). “Deployment of tensegrity structures.” *International Journal of Solids and Structures*, 40(18), 4637–4657.

Sychterz, A. C. and Smith, I. F. C. (2017). “Joint Friction during Deployment of a Near-Full-Scale Tensegrity Footbridge.” *Journal of Structural Engineering*, 143(9), 1–10.

Sychterz, A. C. and Smith, I. F. C. (2018a). “Deployment and shape change of a tensegrity structure using path-planning and feedback control.” *Frontiers in Built Environment*, 4(10), 45–55.

Sychterz, A. C. and Smith, I. F. C. (2018b). “Using dynamic measurements to detect and locate ruptured cables on a tensegrity structure.” *Engineering Structures*, 173(10), 631–642.

Tibert, G. (2002). *Deployable tensegrity structures for space applications*. Royal Institute of Technology.

Veuve, N., Safaei, S. D., and Smith, I. F. C. (2015). "Deployment of a Tensegrity Footbridge." *Journal of Structural Engineering*, 141(11), 1–8.

Veuve, N., Safaei, S. D., and Smith, I. F. C. (2016). "Active control for mid-span connection of a deployable tensegrity footbridge." *Engineering Structures*, 112, 245–255.

Veuve, N., Sychterz, A. C., and Smith, I. F. C. (2017). "Adaptive control of a deployable tensegrity structure." *Engineering Structures*, 152, 10. 14–23.

Xu, X., Sun, F., Luo, Y., and Xu, Y. (2013). "Collision-free path planning of tensegrity structures." *Journal of Structural Engineering*.

Zolesi, V., Ganga, P., Scolamiero, L., Micheletti, A., Podio-Guidugli, P., Tibert, G., Donati, A., and Ghiozzi, M. (2012). "On an innovative deployment concept for large space structures." *42nd International conference on environmental systems (ICES), San Diego, CA, USA*.

Zuk, W. (1968). "Kinetic structures." *Civil Engineering*, 38(12), 62.

List of Tables

	Average control commands for mitigation (cm)				
	Ruptured element				
Deployment length (cm)	Element 26	Element 41	Element 66	Element 69	Variation 2σ
40	3.2	0.6	2.0	2.0	< 0.1
60	5.1	0.8	2.0	2.0	0.1
80	6.2	0.8	2.0	2.0	0.1
100	7.2	0.8	2.4	2.0	< 0.1
120	6.4	0.8	2.0	2.0	< 0.1
140	6.2	1.1	2.4	2.0	0.1
160	6.4	3.4	4.8	4.3	0.2
180	6.2	3.4	4.8	4.3	0.2
200	8.1	3.8	5.3	6.4	0.3

TABLE 1. Average of control commands (cm) of all active cables from the RRT*-connect algorithm for damage mitigation of Elements 26, 41, 66, 69 for the half tensegrity structure. The variation of 2σ is shown for cable-length changes during the five tests of each cable rupture event, averaged over the four cable rupture events.

Deployment length (cm)	Vertical downward displacement after mitigation (mm) Ruptured element			
	Element 26	Element 41	Element 66	Element 69
40		0.9		0.2
60		0.8		0.2
80		0.8		0.4
100		0.9	2.1	0.5
120		0.8	2.2	1.0
140		0.6	2.7	1.7
160	13.3	0.8	3.9	2.3
180	22.7	1.3	18.7	3.7
200	25.3	7.5	20.0	7.4

TABLE 2. Average of measured vertical displacement (mm) of end-nodes after mitigation of rupture of Elements 26, 41, 66, 69 for the half tensegrity structure.

Vector to correct structure	Normalized control commands for active cables 1	 2	 3	 4	 5	 Variation (2σ)
(0,0,1)	0.8	0.9	1.0	0.9	1.0	0.13
(0,1,1)	1.0	1.0	1.0	1.0	0.7	0.21
(0,-1,1)	0.8	0.5	1.0	1.0	0.9	0.26
(1,0,1)	1.0	1.0	1.0	1.0	1.0	0.01
(-1,0,1)	1.0	0.8	0.8	0.8	0.8	0.22
(1,1,1)*	1.0	1.0	1.0	1.0	1.0	–
(-1,1,1)	1.0	1.0	0.8	1.0	0.8	0.24
(1,-1,1)	1.0	0.9	1.0	1.0	1.0	0.17
(-1,-1,1)	1.0	0.7	0.7	1.0	0.7	0.24

TABLE 3. Initial simulated control command entries and correction vectors are shown for damage mitigation of the half tensegrity structure. Vector (1,1,1) marked with a star did not have initial entries. Variation of 2σ of the normalized control commands is shown.

Task	Time per execution (s)	Time required for learning Without CBR	 With CBR
Execution of control commands	2 per cm	5 (cables)*l(cm)	(5 (cables)+ 1/n)*l(cm)
Measure nodal coordinates	10	1	1
RRT*-connect algorithm	∼20	∼1	0
Soft-constraint algorithm	∼300 per cable	5 (cables)	(5/n optional)
Categorize within case-base	0.5	1	1
Mean of entries within case base	0.1	1	1
Normalize control commands and nodal coordinates	0.1	1	1
Compare new entry to case-base	0.5	0	1
Scale selected normalized case	0.1	0	1
Minimum total time		∼1531.3+10l	∼11.3 + 10l+ 2l/n

TABLE 4. Summary of time required per entry for the determination of cable-length changes, l, with no previous information and with case-based reasoning (CBR) is shown. The variable n is the number of entries in the case-base.

	Vector used to correct position of structure			
	Ruptured element			
Deployment length (cm)	Element 26	Element 41	Element 66	Element 69
40		(1,0,1)		(1,0,1)
60		(0,-1,1)		(0,-1,1)
80		(0,0,1)		(0,-1,1)
100		(0,-1,1)	(0,-1,1)	(0,-1,1)
120		(0,0,1)	(0,0,1)	(0,1,1)
140		(0,0,1)	(0,0,1)	(0,0,1)
160	(0,-1,1)	(0,0,1)	(-1,-1,1)	(0,1,1)
180	(0,-1,1)	(0,0,1)	(0,0,1)	(-1,1,1)
200	(0,1,1)	(0,-1,1)	(-1,0,1)	(1,-1,1)

TABLE 5. Vectors used to correct structures from case-base closest to the movement caused by measured rupture events for the half tensegrity structure during deployment.

	Cable-length change (cm)			
	Ruptured element			
Description	Element 26	Element 41	Element 66	Element 69
Mitigation	2.5	2.6	3.4	3.3
Variation (2σ)	0.4	0.2	0.8	0.6

TABLE 6. Average control commands (cm) of all active cables from the RRT*-connect algorithm for damage mitigation of Elements 26, 41, 66, 69 for the connected tensegrity structure. The variation of 2σ is shown for cable-length changes during the five tests of each cable rupture event.

Description	Vertical downward displacement (mm)			
	Ruptured element			
	Element 26	Element 41	Element 66	Element 69
After cable rupture	26.8	16.5	0.4	2.0
After mitigation	11.3	2.6	0.1	1.5
Variation (2σ)	2.4	0.4	0.1	0.3
Relative to serviceability limit of 6.7 mm	4.6	-4.1	-6.6	-5.2

TABLE 7. Average of measured vertical displacement (mm) from end-nodes following the RRT*-connect algorithm for damage mitigation of Elements 26, 41, 66, 69 for the connected tensegrity structure. Variation 2σ is also shown for the five tests of each cable rupture event, averaged over the midspan nodes. The last row shows the performance of mitigation due to each element rupture event compared with the serviceability limit of 6.7 mm.

List of Figures

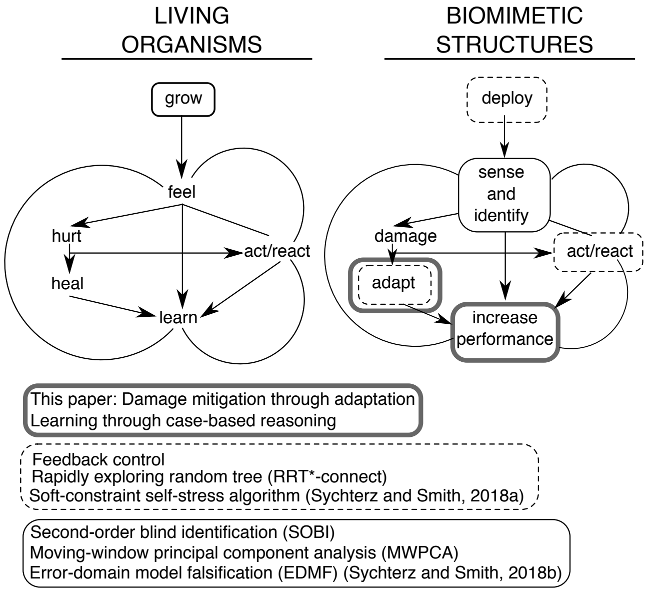

FIG. 1. Scope of this paper, previously developed work, algorithms, and domains of application

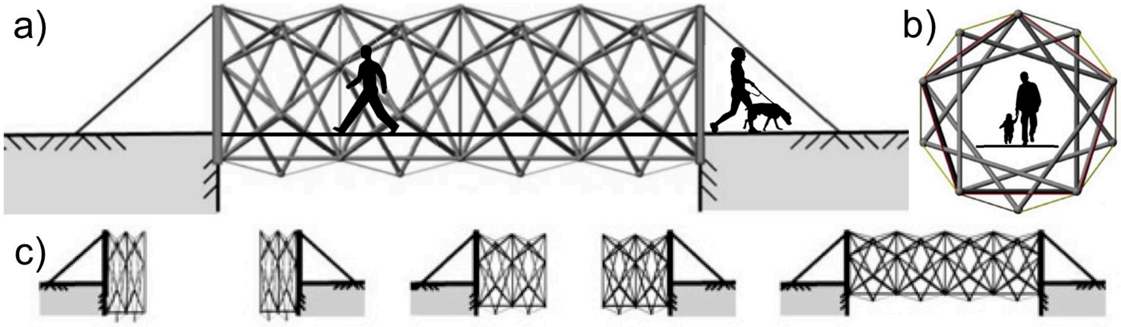

FIG. 2. Side (a) and front (b) views of tensegrity footbridge schematic. Deployment of the structure (c) is shown in three stages.

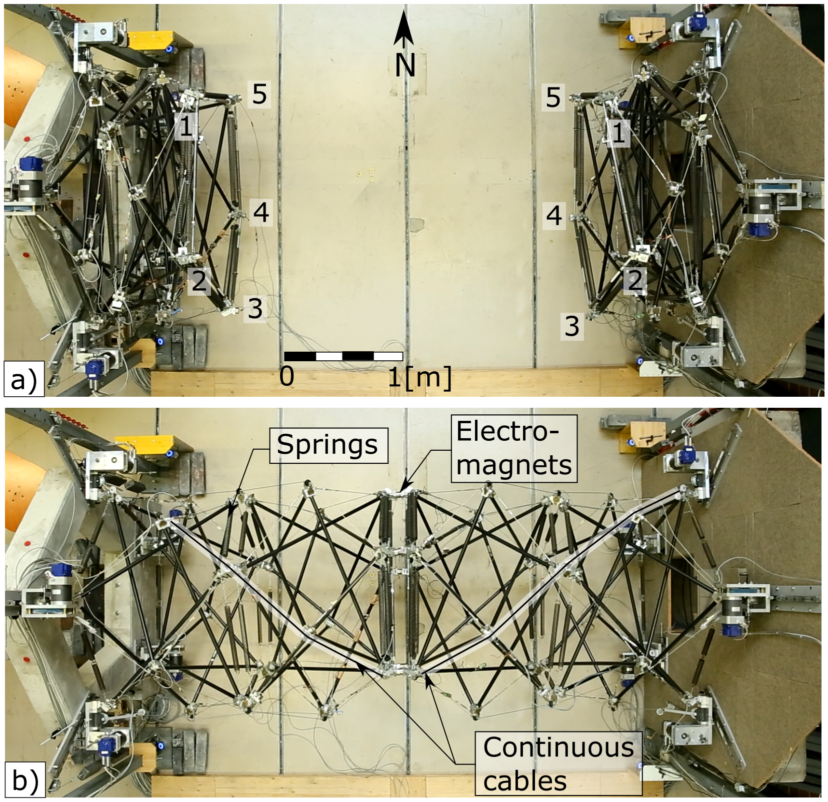

FIG. 3. Top view of folded (a) and connected (b) deployable tensegrity footbridge with continuous cables [Credit: IMAC, EPFL]

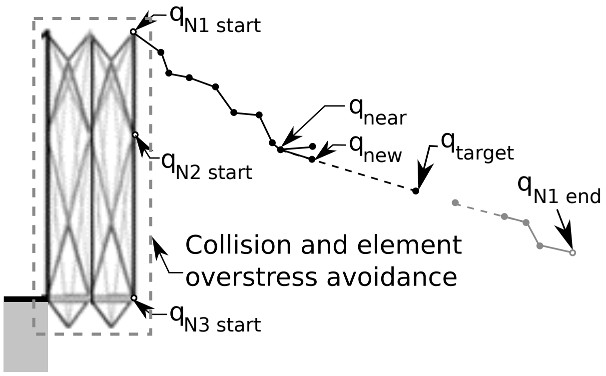

FIG. 4. Path of an end-node is shown for collision and over-stress avoidance. A sample longitudinal 2D-section of the tensegrity structure shows the RRT*-connect algorithm navigation around structural elements in three dimensions. Successful points for two trees, one from the start point and one from the end, are shown in black and grey respectively.

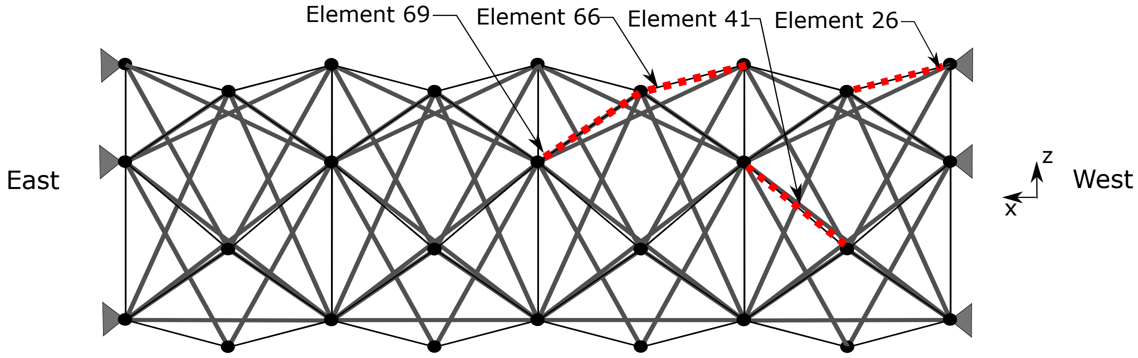

FIG. 5. Elevation sketch of deployed and connected structure. Cables involved in the rupture study (Elements 26, 41, 66 and 69) are shown.

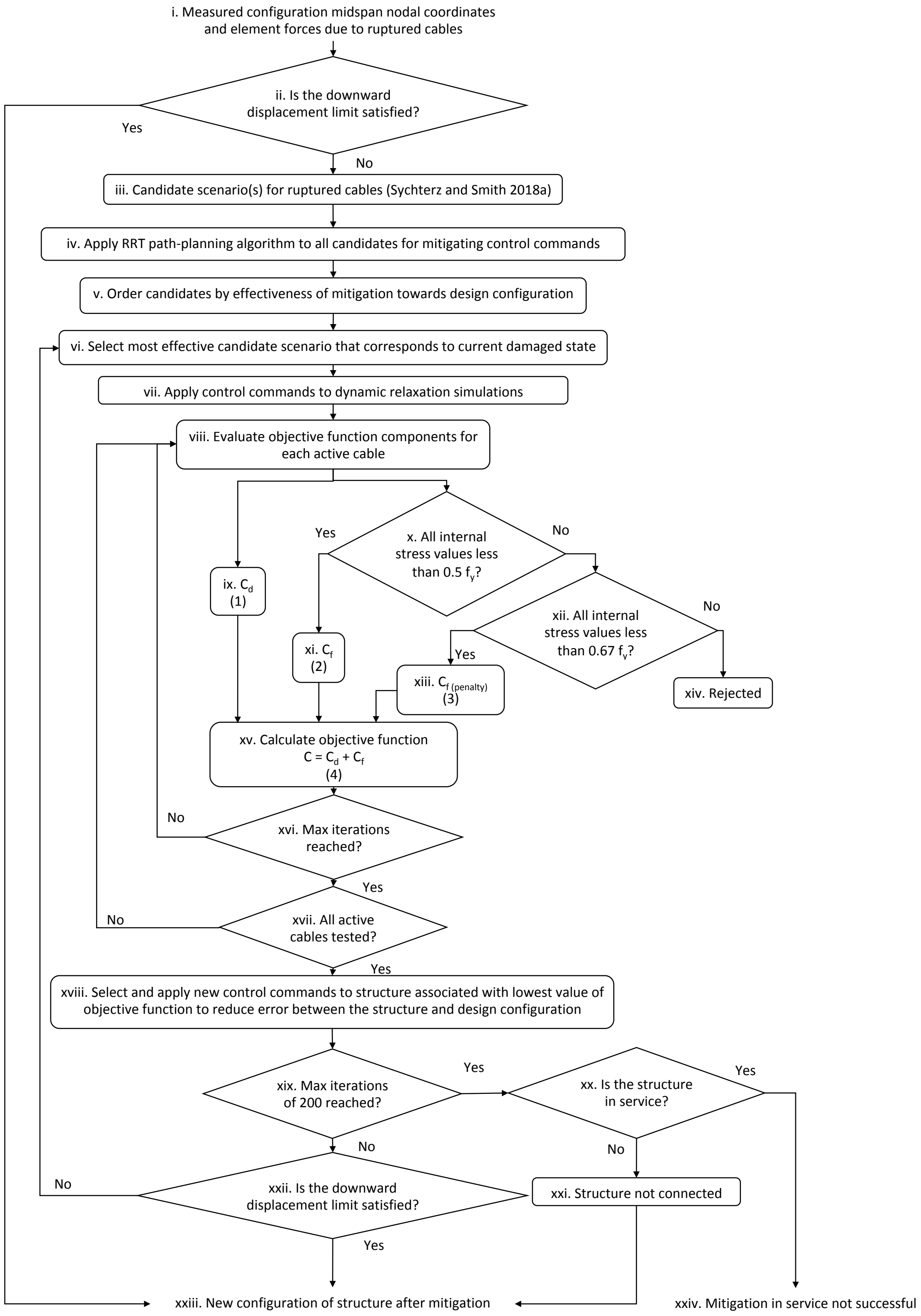

FIG. 6. Procedure for mitigation of the effects of a ruptured element of the tensegrity structure.

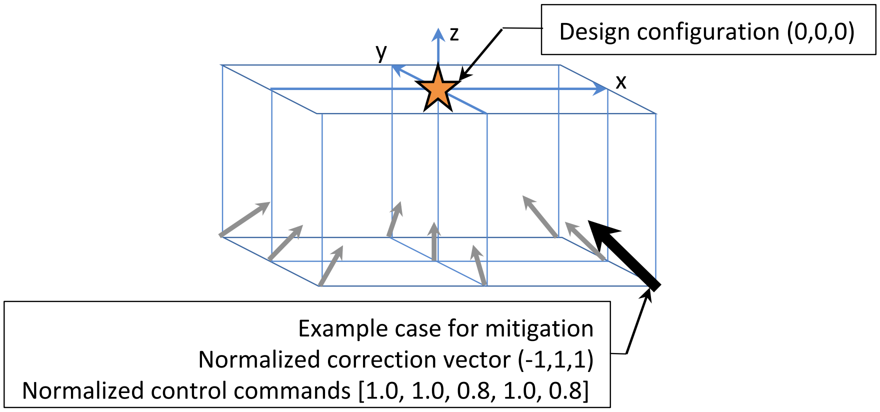

FIG. 7. Schematic of correction vectors for learning using case-based reasoning for mitigation of the tensegrity structure towards the design requirement.

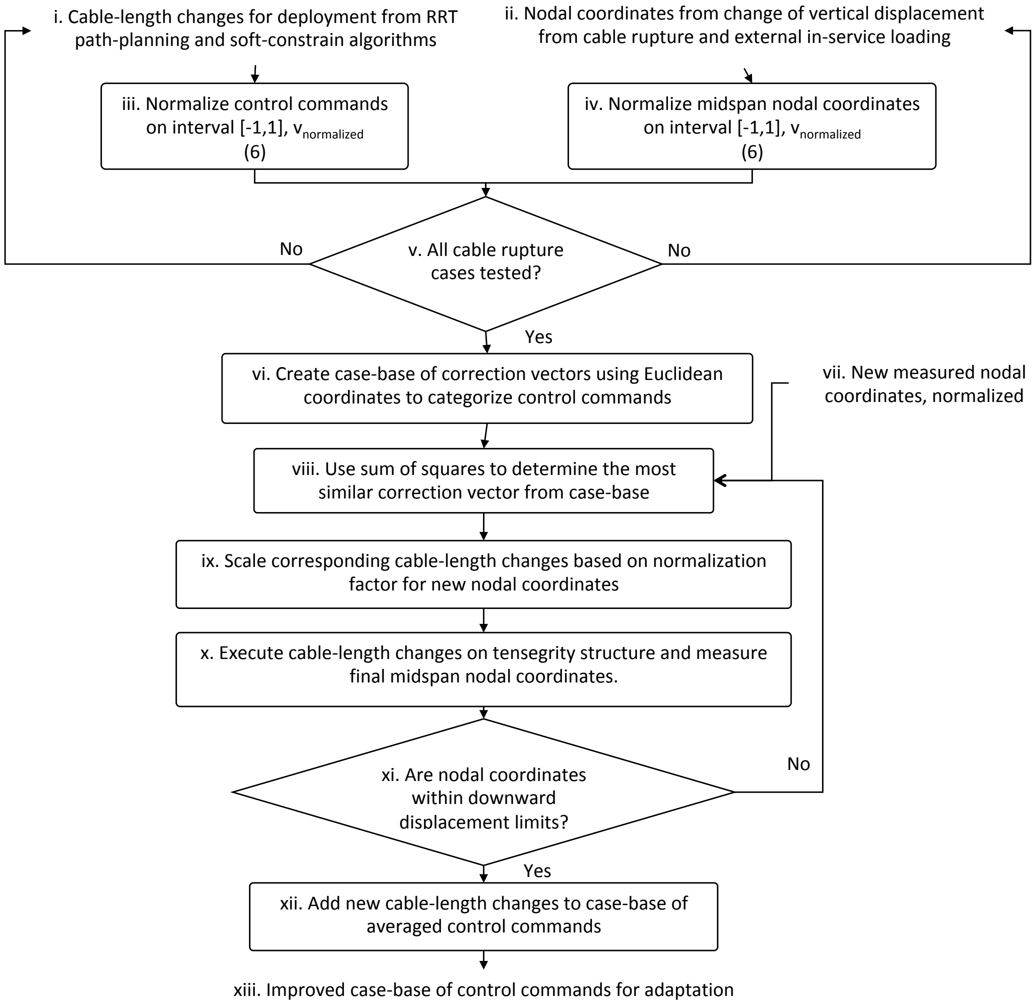

FIG. 8. Procedure following cable rupture of the half tensegrity structure using case-base reasoning.

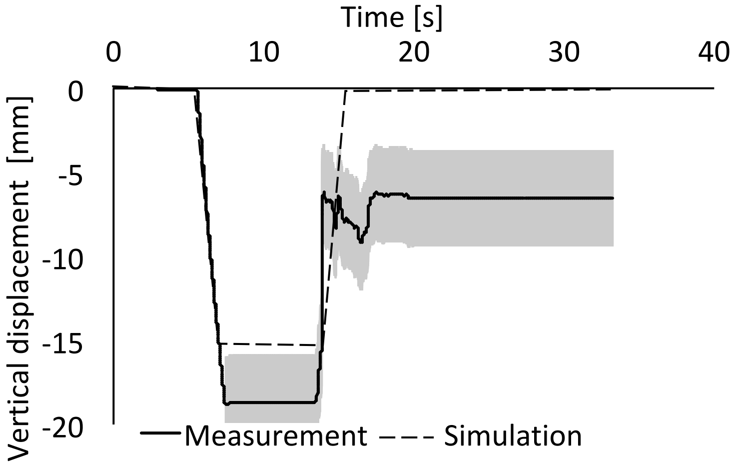

FIG. 9. Vertical displacement of midspan nodes in mm is shown for rupture of Element 41 averaged over five tests with an overall structure length of 140 cm. Measured values are shown with a solid line and the simulated result is shown with a dashed line. Variation of two standard deviations, 2σ, is shown for measurements as a light grey band.

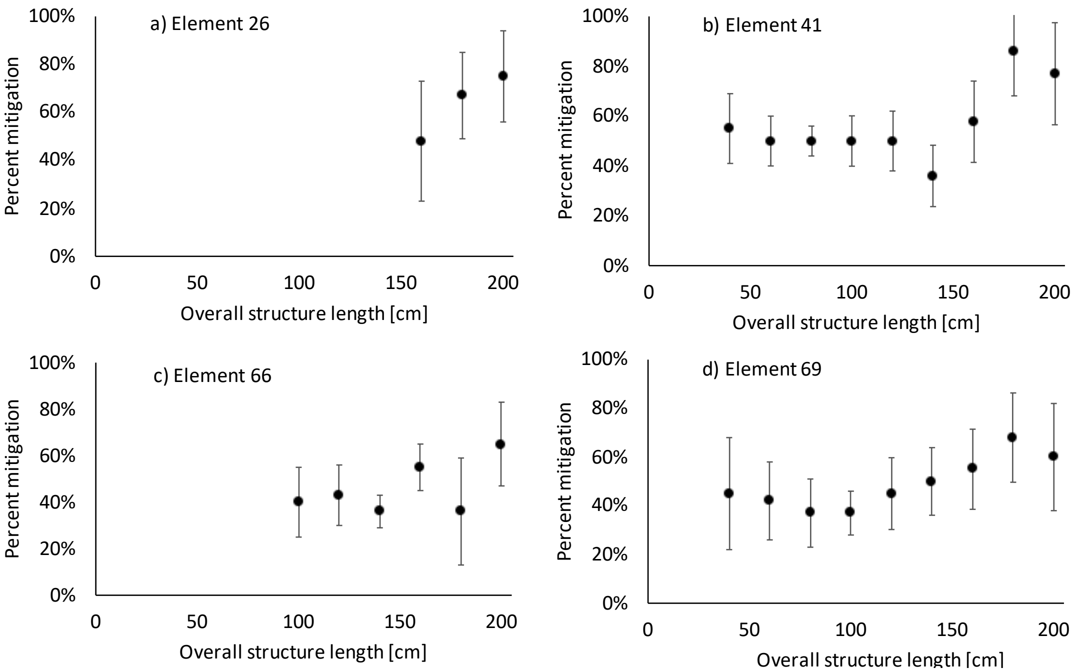

FIG. 10. Percent mitigation for rupture events of Element 26 a), Element 41 b), Element 66 c), and Element 69 d) during deployment.

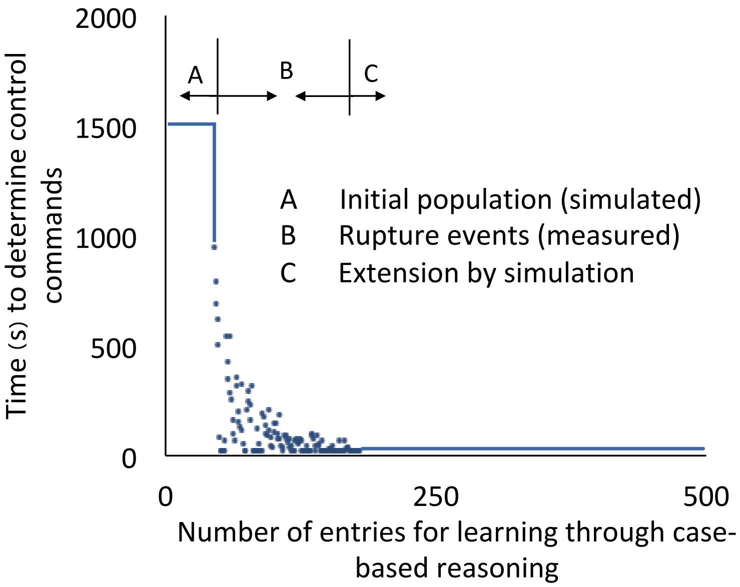

FIG. 11. **Time (s) to determine control commands for deployment of the half tensegrity structure using case-based reasoning implemented following the measurement set.**

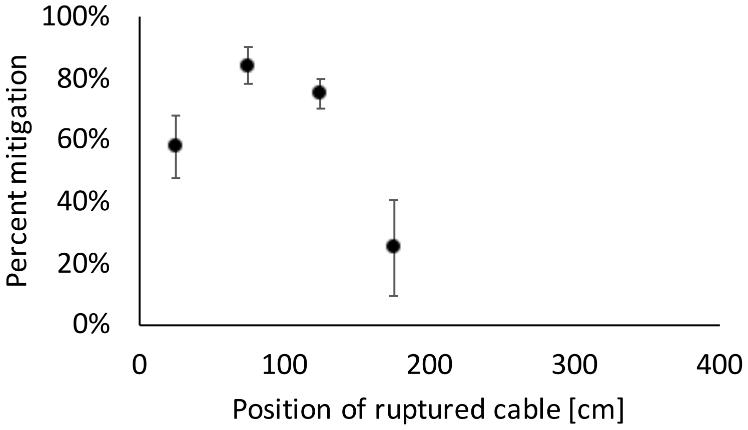

FIG. 12. Percent mitigation of vertical downward displacement for rupture of Element 26, Element 41, Element 66, and Element 69 the connected tensegrity structure.